Article
https://doi.org/10.31489/2024PH4/35-45
UDC 544.42+519.242.7

Received: 06.06.2024
Accepted: 05.08.2024

M.G. Golkovski[1*], I.P. Denisov[2], S.A. Ghyngazov[2], I.P. Vasil'ev[2], I.K. Chakin[1]

[1]Budker Institute of Nuclear Physics, Siberian Branch, Russian Academy of Sciences, Novosibirsk, Russia;
[2]National Research Tomsk Polytechnic University, Tomsk, Russia
*(*Corresponding author's e-mail: golkovski@mail.ru)*

Efficiency of liquid-phase synthesis of ceramic materials under the influence of an electron beam with high penetrating power

The research conducted during of last few years showed the advantages of the method of producing of the luminescence ceramic materials as well as the other purposes ceramics with using of electron beam with high penetrating power. In this technology, an industrial accelerator generates the beam and then it enters the atmosphere throw the hole of small diameter. The accelerating voltage of the electrons is regulated in the range of 1.4 — 2.5 MV, which, in combination with the high beam power, allows for a volumetric effect on the powder material, producing its melting in about 1 s, with virtually no contact between the melt and the walls of the crucible in which the initial batch is placed. The paper proposes a method for calculating the energy efficiency of a beam during the synthesis of two-component oxide ceramics. The measurements show that the beam efficiency is on average about 50 %, and in many cases exceeds 80 %, regardless of the melting temperature of the synthesized ceramics and the heat required to heat and melt it.

Keywords: high voltage electron beam, electron beam output into the atmosphere, electron beam melting, release of beam energy in substances, oxide ceramics synthesis, efficiency of the ceramics synthesis.

1. Introduction

The development of ceramic materials for a specific industry primarily involves synthesis from powder raw materials. The currently used synthesis methods have disadvantages such as long process duration, changes in the stoichiometric composition of the starting components during the synthesis process (ceramic synthesis method), low purity of the synthesized product (co-precipitation method, SHS method), etc. A new method for synthesizing ceramic materials makes it possible to eliminate these shortcomings by activating heating of the initial powder reaction mixtures with a powerful beam of fast electrons. In this method, electrons with energy of more than 1 MeV carry out volumetric heating of the reaction mixture in a short time, ensuring, in addition to a high synthesis rate, high chemical purity, and preservation of the stoichiometric composition and phase homogeneity of the synthesized ceramic materials. These characteristics are especially important in obtaining phosphors [1, 2] and high entropy ceramics, in particular heat-protective ones for creating thermal barrier coating [3] and perovskite structure [4, 5] for solar energetics.

The parameters of electron beams achieved by modern accelerators are sufficient to heat practically any substance in air to the melting point in a time not exceeding a second. This makes possible to carry out the synthesis of ceramic materials in a fast electrons beam under conditions of achieving a liquid-phase state in the reaction mixture. In this case, the efficiency of the synthesis of ceramic materials is the highest, because in the liquid phase the mass transfer in the mixture of reagents is most intense. The combination of high penetrating ability and high beam power allows for the production of ceramic materials with a productivity of 20 kg/h and higher. In a number of works carried out in recent years, V.M. Lisitsyn and co-authors showed that the express synthesis of luminescent ceramics is successfully implemented under conditions of heating the reaction mixture with a powerful beam of fast electrons [6–9]. V.M. Lisitsyn and co-authors beside luminescent ceramics obtained other purpose ceramic materials. Using this method, S.A. Ghyngazov and co-authors synthesized high-entropy ceramic alloys. The last mentioned works conclude that issues of optimizing the conditions of radiation heating should be the subject of special studies.

The aim of this work is to relate the physical characteristics of ceramic powders with the required parameters of their electron beam irradiation modes to achieve the liquid phase of the original powders. The numerical estimates were based on the fact that ceramic powder is a weakly heat-conducting medium, therefore the volumetric heat supply to the material, realized during electron beam processing, will be close to adiabatic. The authors compared two experimental values: the heat required to heat and melt the material according to thermodynamic data and the heat calculated using the irradiation parameters based on the known distribution of the energy release of the electron beam in the material depending on the depth of its penetration. Since this study represents an initial step in obtaining numerical characteristics of the process, it presents the results only for two-component systems. Another reason for choosing only two-component systems is the availability of data on the temperature dependences of enthalpies.

We characterize the energy efficiency of synthesis by a value called beam efficiency, which is understood as the ratio of the energies mentioned above: the energy required to heat and melt the volume of the initial powder material that has passed into a liquid state, and the energy actually introduced into this volume. This coefficient is denoted below by the letter η. When calculating the beam efficiency η, the authors assumed that when an electron beam impacts the powder, the role of radiation effects is negligible, and that the synthesis of ceramics occurs in the liquid phase. If it turns out that radiation plays a significant role in the synthesis, the no-radiation-effect approach is still useful for identifying its contribution.

2. Equipment and experimental procedure

The work was carried out at the Budker Institute of Nuclear Physics of the Siberian Branch of the Russian Academy of Sciences on the “UNU Stand ELV-6” facility. An Industrial accelerator generated a dc current electron beam with an accelerating voltage set in the range of 1.4 — 2.5 MeV. The beam is released into the atmosphere through a 2 mm diameter hole. The distance from the beam release hole to the surface of the material being processed was 9 cm. During the experiments, the values of the electron energy (accelerating voltage) E and the beam current I were established, and the beam power was determined by their product. The beam has a Gaussian distribution of the power flux density in its cross-section. Its Gaussian diameter at a distance of 9 cm from the outlet is approximately 12 mm for electron energy of 1.4 MeV, 10 mm for energy of 2 MeV and 9 mm for energy of 2.5 MeV. Electron beam processing was performed with or without beam scanning. The scanning frequency was 50 Hz. The initial powder was placed in a rectangular massive copper crucible. The internal space of the crucible, where the powder was placed, had dimensions of 50x100xH mm, where the depth H was selected based on the penetrating ability of the beam and the bulk density of the material placed in the crucible and took values of 7, 10 or 14 mm. Initially, the beam was directed to the target to set the required parameters. Then the crucible began to move under the beam, moving along its length perpendicular to the beam scanning direction at a speed of 1 cm/s. In the beam scanning mode, the entire surface of the powder placed in the crucible was processed, for which the scanning span was set equal to the crucible width l=5 cm. In the non-scanning mode, a processed track with a width comparable to the beam diameter was formed in the material layer.

During the experiments, a parameter called the mass thickness of the processed material σ was monitored. It was determined by the formula:

$$\sigma = \frac{m}{S}, \tag{1}$$

where m is the mass of the material in the crucible, S is the area of its bottom. Three types of mass m were recorded: the mass of the material before irradiation, the mass of the contents of the crucible after irradiation, and the mass of the ceramics synthesized because of irradiation. Accordingly, three mass thicknesses were recorded: σ_1, σ_2 and σ_{melt}. Obviously, the mass thickness of ceramics makes sense and was determined only in scanning modes.

3. Calculation formulas
3.1. Definition of the term beam efficiency in this paper

As stated in the Introduction, by beam efficiency η we mean the ratio of the heat required to melt the synthesized volume of ceramics to the heat introduced by the beam into this volume. The value of η can be determined by the formula:

$$\eta = \frac{h_{melt}}{w_{melt}}, \tag{2}$$

where h_{melt} is the energy required to heat 1 g of material from room temperature to the melting point and then melt it at this temperature, w_{melt} is the value of energy actually introduced in 1 g of molten material.

The heat required to melt ceramic powders was determined based on thermodynamic databases [10, 11, 12] as the difference between the enthalpies of the molten material at the melting temperature and the material in the initial state at room temperature according to the formula:

$$h_{melt} = \frac{H_{liq}\ \ T_{пл}\ \ - H_{sol}\ \ 300K}{M}\ , \tag{3}$$

where $H_{liq}(T_{пл})$ and $H_{sol}(300K)$ are molar enthalpies of material at liquid state at melting temperature and solid state at room temperature, M is molar mass in g. The amount of energy expended per 1 g of ceramics w_{melt} is determined based on the parameters of the irradiation mode and the known distributions of energy release by electrons according to the depth of their penetration into the material.

3.2. Calculation of expended beam energy w_{melt}.

As was indicated in Section 2, the beam has a non-uniform Gaussian distribution of the power flux density in its cross-section. Its Gaussian diameter is comparable to the depth of beam penetration into the powder material. However, when scanning the beam with simultaneous movement of the crucible in the direction perpendicular to the scanning, we obtain a large surface area, almost simultaneously processed by the beam. The distribution of energy released inside the material will be close to that which would be observed from a wide beam with a uniform distribution of the power flux density over the area of its cross-section. The size of this cross-section in the scanning direction coincides with the scanning span, i.e. is equal to approximately 5 beam diameters. In the direction perpendicular to scanning, it is equal to at least 2...3 beam diameters, since due to the poor thermal conductivity of the ceramic powder, the heat is retained in the volume where it was introduced for a noticeable time. During this time, the crucible has time to move several beam diameters. Based on the above, the beam can be considered wide, with a uniform distribution of the power flow over its cross-section and dimensions that are many times greater than the depth of its penetration. The problem of energy loss distribution in the material for such beams can be considered one-dimensional.

For wide beams, the distribution of energy release by accelerated electrons by the depth of their penetration into the material depending on the initial electron energy E and the composition of the material has been studied many times. T. Tabata et al. presented these results in analytical form in a number of works, in particular [13, 14]. Figure 1 presents the distributions constructed on the basis on the indicated works for some characteristic modes for which measurements were performed in this work. The ordinate axis of the distributions shows the mass thickness of the material z in g/cm^2, measured from the powder surface. The abscissa axis shows the derivative of the electron energy E (in MeV) with respect to z. The $\frac{-}{\mathrm{dz}}\frac{dE}{dz}$ value characterizes the intensity of energy losses by electrons in the material and is measured accordingly in ——— ———. In the graphs in Figure 1, to the left of the vertical axis, after the chemical formulas of the processed substances, the initial energies of electrons in MeV are given in brackets in the second position. The presented distributions can only be used to calculate the energy release inside materials during beam scanning processing. They are not applicable to narrow beam processing without scanning.

If the ceramic synthesis occurs in a certain layer of powder from depth z_1 to z_2, the mass thickness of the melt is equal to $\sigma_{melt} = z_2 - z_1$. The energy loss per electron in MeV when passing from layer z_1 to layer z_2 will be $-\int_{z_1}^{z_2}\frac{dE}{dz}dz$. The beam power released between layers with coordinates z_1 and z_2 is equal to $P = \int_{z_1}^{z_2}\frac{dE}{dz}dz \cdot I$, where I is the beam current. The mass of ceramics melted in 1 s is equal to $\sigma_{melt} \cdot l \cdot v$, where σ_{melt} is the mass thickness of the melted ceramics, l is the width of the scanning, v is the speed of movement of the crucible under the beam. Dividing the power spent on melting the ceramics by the mass of the ceramics obtained in 1 s gives the beam energy consumption per unit mass of the ceramics:

$$w_{melt} = \frac{\int_{z_1}^{z_2}\frac{dE}{dz}dz \cdot I}{\sigma_{melt} \cdot l \cdot v} = \frac{\left(\frac{dE}{dz}\right)_{mid} \cdot I}{l \cdot v}\ , \tag{4}$$

where $\left(\frac{dE}{dz}\right)_{mid}$ is the average value of the intensity of energy loss by each electron in the region between z_1 and z_2.

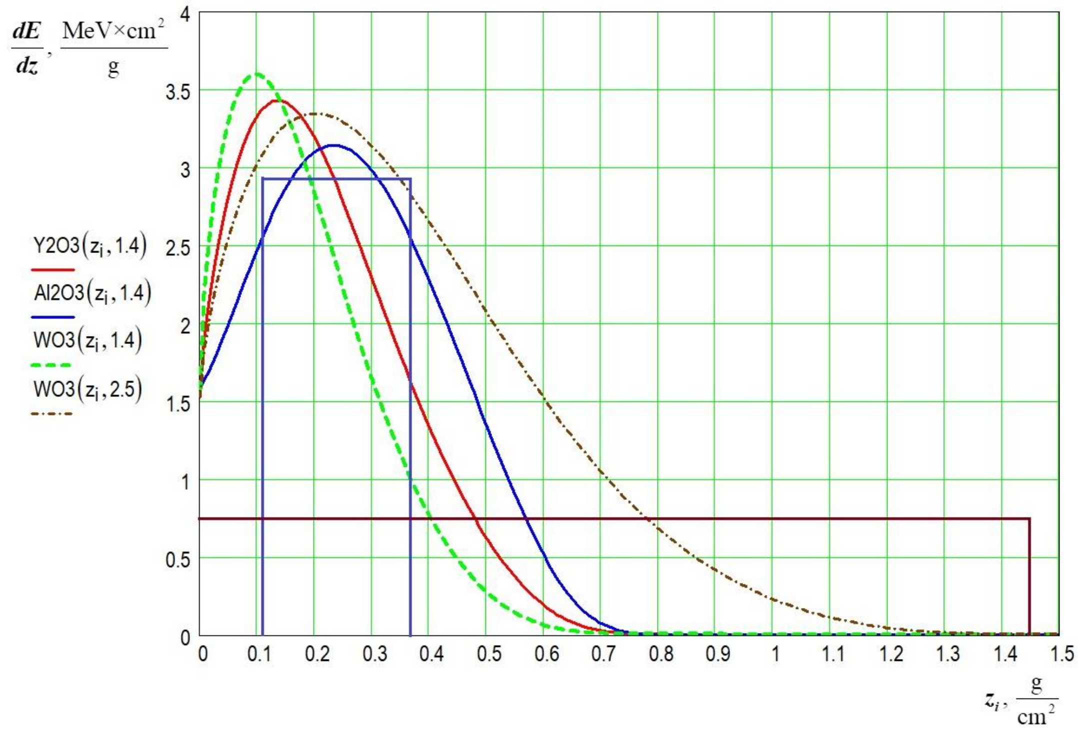

Figure 1. Distributions of electron energy losses as a function of mass thickness, normalized to one electron. The distributions represent the characteristic modes given in Table 1

In Figure 1, as an example, the vertical lines indicate the values of z_1 and z_2 for samples synthesized from Al_2O_3 and WO_3 powders. For a sample of WO_3, z_1=0. The horizontal lines for these samples indicate the average values of the intensity of energy losses. In the case where the mass thickness of the melt layer σ_{melt} approaches or exceeds the mass thickness of beam penetration, the energy expended on melting will be equal to the entire energy introduced by the beam, since the absorption of the beam energy will occur entirely in the melt. Then the entire beam power P, with the exception of the power carried away by reflected electrons and bremsstrahlung, will be introduced into the melt and the efficiency can be written using a simpler formula, representing w_{melt} as

$$w_{1melt} = \frac{1-\gamma\ Pt}{m_{melt}}, \tag{5}$$

and beam efficiency in this case will be equal:

$$\eta_1 = \frac{h_{melt} m_{melt}}{1-\gamma\ Pt}, \tag{6}$$

where P is the beam power; γ is the beam reflection coefficient by power, the reflection coefficient γ depends on the composition of the substance and is close to 0.1; t is the time it takes for the crucible to pass under the beam, in the experiments it is equal to 10 s; h_{melt} is the energy required to heat and melt 1 g of material; m_{melt} is the mass of the melt.

If the mass thickness of the melt is noticeably less than the beam penetration depth, formula (4) must be used, since (6) will give underestimated beam efficiency values.

When conducting experiments without scanning, the beam cannot be considered wide. The calculation of the expended energy according to (4), using the distribution for wide beams, is incorrect. However, formula (6) remains valid, since it does not use the distribution of energy losses by depth. It is only necessary that the condition of exceeding the mass thickness of the powder fill compared to the beam penetration depth be met. In addition, it should be borne in mind that in threshold modes without scanning, at low powers corresponding to the beginning of the melt appearance, formula (6) will give underestimated values of the beam efficiency.

4. Results and Discussion

During the work, a synthesis was carried out and the beam efficiency was calculated for several dozen samples from different materials with and without beam scanning under different irradiation parameters. In order to reduce the volume of the article, the authors selected 11 characteristic modes with scanning (Table 1) and 7 modes without scanning (Table 2) for analysis. The samples in the tables are arranged in order of increasing energy h_{melt} required for their heating and melting. Figure 2 shows the appearance of some samples from Table 1, Figure 3 — from Table 2.

4.1. Modes with scanning of the beam.

It should be noted that the data on the modes for Y_2O_3, Al_2O_3 (405), MgF_2, BaF_2 presented in Table 1 are quite reliable, since they have been confirmed by 4–8 experiments under similar conditions for each of the substances. The first column of Table 1 indicates the powder material and (in brackets) their marking according to the laboratory classification. Remaining columns use the following designations:

$T_{пл}$ — melting point of the material;
h_{melt} — the energy required to heat and melt 1 g of material (see (3));
E — energy (accelerating voltage) of beam electrons;
P — beam power;
Powder scattering — loss of mass of crucible contents during irradiation in %;
σ_2 — mass thickness of the crucible contents after irradiation (melt + remaining powder);
σ_{melt} — mass thickness of the melt;
η — beam efficiency coefficient calculated according to (2).

Table 1

Processing modes with scanning of the beam

Composition and marking of powder	$T_{пл}$, °C	h_{melt}, kJ/g	E, MeV	P, kW	Powder scatter, %	σ_2, g/cm^2	σ_{melt}, g/cm^2	Beam efficiency, η
BaF_2 (520)	1368	0.905	1.4	16	0.5 %	1.55	1.52	0.53
WO_3 (438)	1472	0.935	1.4	16	3.4 %	1.74	1.45	0.56
WO_3 (439	1472	0.935	2.5	24	35 %	1.31	0.93	0.24
MgF_2 (516)	1263	0.942	1.4	15	0.4 %	0.85	0.84	0.27
Ga_2O_3 (474)	1807	1.75	1.4	17	0.8 %	1.06	1.06	0.61
SiO_2 (sand)	1600	1.87	2	17	1.4 %	1.01	0.59	0.42
Y_2O_3 (490)	2439	2.05	1.4	25	1.3 %	1.11	1.03	0.47
Al_2O_3 (816)	2054	3.5	1.4	10	0.1 %	0.94	0.26	0.84
Al_2O_3 (413)	2054	3.5	1.4	26	0.8 %	0.98	0.88	0.61
Al_2O_3 (sand)	2054	3.5	2	24	0.1 %	1.02	0.78	0.63
MgO (485)	2832	5.66	1.4	25	5.7 %	0.51	0.49	0.63

Appearance of synthesized ceramics in the modes with beam scanning. Figure 2 a and b show the "borderline" mode, in which the synthesis of ceramics in the thickness of the material under the surface of the powder is just beginning. As a result, in the Al2O3 (816) mode, a thin plate was formed lying under a layer of powder. During the cleaning process, it broke into separate fragments. Figure 2b shows them joined in their original form. The remaining photos show samples with the melt reaching the surface of the powder. After solidification, the melt is either flat drops that can merge to form plates (Fig. 2 c), or merged rollers oriented along the beam scanning direction (Fig. 2 d), or thickened plates with smooth surfaces (Fig. 2 e, f, h). Fig. 2 g, h shows a sample obtained from coarse-dispersed material in the form of quartz sand of technical purity with a particle size of up to 500 µm. As can be seen from Table 1, the large particle size is not a factor that significantly reduces the beam efficiency.

Beam efficiency in the modes with scanning of electron beam. In their calculations, the authors assumed that the synthesis of ceramics occurs in a layer of a certain thickness. In most cases, the melt is formed from the surface of the powder bed $z_1=0$ to a certain depth, $z=\sigma_{melt}$. This situation is observed for all samples presented in Table 1, with the exception of the Al_2O_3 (816) sample (Fig. 2 a, b). As indicated in section 3.2, in the graphs of Figure 1, as an example, for samples of Al_2O_3 (816) and WO_3 (438) the melt boundaries and average values of electron energy losses in the melt thickness — — — are indicated. The melt thickness of the WO_3 (438) sample significantly exceeds the beam penetration depth. This means that heat transfer from the beam-heating zone to the underlying melt layers occurred due to convection in the melt.

a) Al2O3 (816), appearance after irradiation, σ2=0.94 g/cm2

b) Al2O3 (816), σmelt=0.26 g/cm2

c) Ga2O3 (474), σ2=1.06 g/cm2

d) MgO (485), σ2=0.51 g/cm2

e) MgF2 (516), σ2=0.85 g/cm2

f) Y2O3 (490), σ2=1.03 g/cm2

g) SiO2 before treatment sand, σ2=1.01 g/cm2

h) SiO2 after treatment sand, σmelt=0.59 g/cm2

Figure 2. Appearance of samples after scanning beam treatment:
a, c, d, e, f — appearance of samples after irradiation, b — fragments of synthesized plate of Al_2O_3 (816), g — SiO2 sand before treatment and h — ceramic plate synthesized from it, raised above the crucible

In a number of modes, low electron beam efficiency is observed, down to 0.2. Such modes usually occur under the following circumstances:

— The mass thickness of the initial powder is noticeably less than the beam penetration depth, due to which the melt reach the bottom of the crucible, and a noticeable part of the heat leaks into the thick-walled copper bottom of the crucible.

— The beam power exceeds that required to melt the powder placed in the crucible. For example, in the MgF_2 (516) mode, the surface density of the introduced energy required to melt the powder should be $0.84 g/cm^2 \cdot 0.942 kJ/g = 0.79 kJ/cm^2$. Taking into account the beam efficiency, for example, 0.5, this value can increase to 1.6 kJ/cm^2. In reality, the specific energy introduced was $15 kW/5 cm^2/s = 3 kJ/cm^2$, which resulted in the melt touching the bottom of the crucible (Fig. 2e).

— There is observed a noticeable scattering of the original powder during the irradiation process, for example, in the WO_3 mode (439). The reasons for the scattering have not been precisely determined. These may include: the presence of volatile impurities in the powder, which can cause both the powder to fly apart and small droplets of melt to splash; the nano-sized range of powder particles; electrification of powder particles when irradiated with electrons. Due to their low bulk density, nano-sized powders cannot be placed in a crucible with sufficient mass thickness. In addition, the thickness of the nanopowder contains a large volume of air, which, when heated, expands and can cause the powder to scatter. The acceptable powder particle size is 5–500 μm. The influence of electrification has not been confirmed, since high efficiency modes are observed on some high-purity dielectric powders (see modes with Al_2O_3 and MgO in Table 1). In the case of the WO_3 (439) sample, the reason for the large spread and low efficiency could have been the combination of an excess (at least 2 times greater than necessary) beam power with an increased penetration depth. In the photo of this sample after irradiation (not included in the article), one can see the scattering of powder and small drops of melt beyond the crucible.

4.2. Processing modes without beam scanning.

In Table 2 which presents the characteristic modes without beam scanning (track modes), the following designations are used:

h_{melt} — the energy required to heat and melt 1 g of material (see (3));

P — beam power;

E — energy (accelerating voltage) of beam electrons;

m_{melt} — mass of sintered (molten) material in a crucible;

Powder scattering — the loss of powder mass during irradiation in g;

σ_2 — mass thickness of the crucible contents after beam processing;

η_1 — efficiency coefficient (6), in the calculation of which the expended energy (5) is defined as the total energy introduced by the beam minus the energy reflected from the surface of the material.

Table 2

Processing modes without scanning of the beam

Composition and marking of powder	$T_{пл}$, °C	h_{melt}, kJ/g	P, kW	E, MeV	m_{melt}, g	Powder scatter, g	σ_2, g/cm^2	Beam efficiency η_1
BaF_2 (518)	1368	0.905	4	1.4	22.29	1.24	1.69	0.64
WO_3 (437)	1472	0.935	4	1.4	25.63	0.49	1.6	0.82
MgF_2 (515)	1263	0.942	4	1.4	19.09	0.13	0.92	0.46
Ga_2O_3 (473)	1807	1.75	4	1.4	15.25	0.21	1.1	0.75
Y_2O_3 (489)	2439	2.05	4	1.4	10.24	0.42	1.18	0.61
ZnO (468)	1977	2.15	4	1.4	12.39	0.62	0.50	0.75
Al_2O_3 (405)	2054	3.5	4	1.4	9.43	0.24	0.82	0.85
MgO (484)	2832	5.66	7	1.4	9.79	0.2	0.58	0.82

a) Ga2O3 (473), σ2=1.1 g/cm2, η=0.75

b) Y2O3 (489), σ2=1.18 g/cm2, η=0.61

c) ZnO (468), σ2=0.50 g/cm2, η=0.75

d) MgO (484), σ2=0.58 g/cm2, η=0.82

e) Al2O3 (405), σ2=0.82 g/cm2, η=0.85

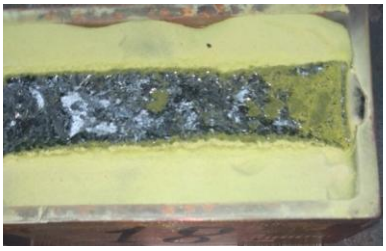

f) WO3 (437), σ2=1.6 g/cm2, η=0.82

Figure 3. Appearance of samples after processing without beam scanning (in track mode)

All modes in Table 2, with the exception of ZnO (468), Al_2O_3 (405) and MgO (484), are performed on the same materials as the modes in Table 1, so that when comparing modes with and without scanning, the material influence factor is excluded. Comparison of the efficiency of η and η_1 in Table 1 and Table 2 shows that the energy input efficiency in modes without scanning is higher. This seems strange and requires a separate discussion.

The beam is non-uniform in cross section. The maximum power flux density is realized near the beam axis. As you move away from the axis, it decreases approximately according to Gauss's law. The movement of the material under a stationary beam leads to the formation of a melting track in it. The power flux density at some distance from the beam axis is already insufficient to melt the material. That is, part of the beam power is spent on heating the edges of the track without melting them. When scanning the beam, the power flux density is averaged across the scanning area and the edge zones of the beam contribute to the averaged power flux density, as a result of which the entire beam power is utilized and, it would seem, the efficiency during scanning should be higher.

In practice, we observe the opposite picture. The explanation seems to be as follows: In the non-scanning mode, the maximum beam energy is released on the axis of the melting track on some depth under the surface of treated material. In the region of maximum energy release, the beam overheats the melt above the melting temperature. Due to convection and thermal conductivity inside the melt, the temperature spreads from the central region of the melt to the periphery, heats it, and powder particles are drawn into the zone of overheated melt and in turn melt. Thus, the size of the melt zone becomes larger than the zone heated by the beam to the melting temperature. In modes with scanning, the situation is different. Thermal insulation is worse. Either plates or large drops are formed. They come into contact with the powder mainly only from below. The relative amount of peripheral powder entering the overheated zone of the melt is less.

Conclusions

1. Accelerated synthesis of ceramics under the influence of an electron beam for two-component oxides can be explained by the formation of a liquid phase according to an equilibrium thermodynamic mechanism without taking into account radiation effects. The energy introduced by the electron beam is more than enough to melt the powder material.

2. The method for producing ceramics using an electron beam with MeV-range electron energy is characterized by high beam energy efficiency, which is expressed through the beam efficiency coefficient η proposed in this work. Its average value, regardless of the energy required to melt the material and the melting temperature, exceeds 50 %, and in some cases, the beam efficiency exceeds 80 %.

3. For most of the studied substances, the loss of powder mass during the synthesis process does not exceed several percent.

4. Efficiency values less than one third are observed in the following cases:

- during processing, significant powder dispersion occurs;
- the selected beam power significantly exceeds that required to melt the material placed in the crucible;
- the mass thickness of the initial powder layer is less than the mass thickness of the beam penetration.

Acknowledgments

The work was supported by the Russian Science Foundation, grant No. 23-79-00014.

References

1 Lv, Xiang et al. Recent progress on modulating luminescence thermal quenching properties of bi3+-activated phosphors / Xiang, Lv et al. // Inorganic Chemistry Frontiers. — 2024. — Vol. 11. — No. 6. — P. 1668–1682. https://doi.org/10.1039/d3qi02588h.

2 Haider, Asif Ali, et al. Advances in reversible luminescence modification and applications of inorganic phosphors based on Chromism reaction / Asif Ali, Haider // Advanced Optical Materials. — 2023. — Vol. 12. — No. 5. https://doi.org/10.1002/adom.202302265.

3 Zhou, Ming et al. Reaction mechanisms of (re0.2nd0.2sm0.2eu0.2gd0.2)2zr2o7 (re = la or YB) under Cao-MgO-Al2O3-SiO2 (cmas) attack / Ming, Zhou et al. // Journal of the European Ceramic Society. — 2024. — Vol. 44. — No. 6. — P. 4055–4063. https://doi.org/10.1016/j.jeurceramsoc.2024.01.014.

4 Li, Xudong et al. Enhanced redox electrocatalysis in high-entropy perovskite fluorides by tailoring D–P hybridization / Xudong, Li et al. // Nano-Micro Letters. — 2023. — Vol. 16. — No. 1. https://doi.org/10.1007/s40820-023-01275-3.

5 Wang, Yuhao et al. High-entropy perovskites for Energy Conversion and storage: Design, synthesis, and potential applications / Yuhao, Wang et al. // Small Methods. — 2023. — Vol. 7. — No. 4. https://doi.org/10.1002/smtd.202201138.

6 Lisitsyn, Victor, et al. Radiation synthesis of high-temperature wide-bandgap ceramics / Victor, Lisitsyn et al. // Micromachines. — 2023. — Vol. 14. — No. 12. — P. 2193. https://doi.org/10.3390/mi14122193.

7 Lisitsyn, Victor et al. The optimization of Radiation Synthesis Modes for YAG: CE Ceramics / Victor, Lisitsyn et al. // Materials. — 2023. — Vol. 16. — No. 8. — P. 3158. https://doi.org/10.3390/ma16083158.

8 Lisitsyn, Victor et al. Express synthesis of YAG: CE ceramics in the high-energy electrons flow field / Victor, Lisitsyn et al. // Materials. — 2023. — Vol. 16. — No. 3. — P. 1057. https://doi.org/10.3390/ma16031057.

9 Ghyngazov, S.A. et al. Synthesis of technical ceramics in a beam of fast electrons / S.A. Ghyngazov // Russian Physics Journal. — 2023. — Vol. 66. — No. 4. — P. 391–397. https://doi.org/10.1007/s11182-023-02952-x.

10 NIST Chemistry Webbook, SRD 69. Chemical Formula Search. — [Electronic resource]. — Access mode: webbook.nist.gov/chemistry/form-ser/. Accessed 16 Oct. 2024.

11 Глушко В.П. (ред.). Термодинамические свойства индивидуальных веществ: Справоч. изд.: [В 4-х т.]. — 3-е изд. / В.П. Глушко (ред.), Л.В. Гурвич и др. — М.: Т. 1 — 1978; Т. 2 — 1979; Т. 3 — 1981; Т. 4 — 1982.

12 Термодинамические свойства индивидуальных веществ: Справоч. изд. — Т. 5 (онлайн версия). — [Электронный ресурс]. — Режим доступа: https://www.chem.msu.su/rus/tsiv/

13 Tabata, Tatsuo et al. An algorithm for depth–dose curves of electrons fitted to Monte Carlo data / Tatsuo, Tabata // Radiation Physics and Chemistry. — 1998. — Vol. 53. — No. 3. — P. 205–215. https://doi.org/10.1016/s0969-806x(98)00102-9.

14 Tabata, Tatsuo et al. (1994). Energy deposition through radiative processes in absorbers irradiated by electron beams / Tatsuo, Tabata // Nuclear Instruments and Methods in Physics Research Section B: Beam Interactions with Materials and Atoms. — Vol. 93. — No. 4. — P. 447–456, https://doi.org/10.1016/0168-583x(94)95633-2.

М.Г. Голковский, И.П. Денисов, С.А. Гынгазов, И.П. Васильев, И.К. Чакин

Жоғары ену қабілеті бар электронды сәуленің әсерінен керамикалық материалдардың сұйық фазалық синтезінің тиімділігі

Соңғы бірнеше жылда жүргізілген зерттеулер люминесцентті керамикалық материалдарды, сондай-ақ жоғары ену қабілеті бар электронды сәулені қолданатын басқа мақсаттағы керамиканы алу әдісінің артықшылықтарын көрсетті. Сәулені өнеркәсіптік электронды үдеткіш жасайды және атмосфераға шағын диаметрлі тесік арқылы шығарылады. Электрондардың үдеткіш кернеуі 1,4 – 2,5 МВ диапазонында реттеледі, бұл сәуленің жоғары қуатымен бірге ұнтақ материалға көлемдік әсер етуге мүмкіндік береді, оны шамамен 1 с уақыт ішінде балқытады, яғни балқыманың бастапқы шихта орналасқан тигель қабырғаларымен жанасуынсыз. Жұмыста екі компонентті оксидті керамиканы синтездеу кезінде сәуленің энергетикалық тиімділігін есептеу әдісі ұсынылған. Сәуленің тиімділігі синтезделген керамиканың балқу температурасына және оны қыздыру мен балқыту үшін қажет жылуға қарамастан, орташа есеппен 50% құрайды және көптеген жағдайларда 80%-дан асады.

Кілт сөздер: жоғары вольтты электронды сәуле, электронды сәулені атмосфераға шығару, электронды сәулені балқыту, заттардағы сәулелік энергияны бөлу, оксидті керамика синтезі, керамика синтезінің тиімділігі.

М.Г. Голковский, И.П. Денисов, С.А. Гынгазов, И.П. Васильев, И.К. Чакин

КПД жидкофазного синтеза керамических материалов под воздействием электронного пучка с высокой проникающей способностью

Проведённые в последние несколько лет исследования показали преимущества метода получения люминесцентных керамических материалов, а также керамик другого назначения с применением электронного пучка с высокой проникающей способностью. Пучок генерируется промышленным ускорителем электронов и выпускается в атмосферу через отверстие малого диаметра. Ускоряющее напряжение электронов регулируется в диапазоне 1,4–2,5 МВ, что в сочетании с высокой мощностью пучка позволяет оказывать объёмное воздействие на порошковый материал, производя его расплавление за время около 1 с, практически без соприкосновения расплава со стенками тигля, в который помещается исходная шихта. В статье предложен способ расчёта энергетического КПД воздействия пучка при синтезе двухкомпонентных оксидных керамик. Показано, что КПД пучка в среднем составляет около 50 %, а во многих случаях превышает 80 %, вне зависимости от температуры плавления синтезируемой керамики и тепла, необходимого для её нагрева и расплавления.

Ключевые слова: высоковольтный электронный пучок, вывод электронного пучка в атмосферу, электронно-лучевая плавка, выделение энергии пучка в веществах, синтез оксидной керамики, КПД синтеза керамики.

References

1 Lv, Xiang et al. (2024). Recent progress on modulating luminescence thermal quenching properties of bi3+-activated phosphors. *Inorganic Chemistry Frontiers, 11*(6), 1668–1682. https://doi.org/10.1039/d3qi02588h.

2 Haider, Asif Ali, et al. (2023). Advances in reversible luminescence modification and applications of inorganic phosphors based on Chromism reaction. *Advanced Optical Materials, 12*(5). https://doi.org/10.1002/adom.202302265.

3 Zhou, Ming et al. (2024). Reaction mechanisms of (re0.2nd0.2sm0.2eu0.2gd0.2)2zr2o7 (re = la or YB) under Cao-MgO-Al2O3-SiO2 (cmas) attack. *Journal of the European Ceramic Society, 44*(6), 4055–4063. https://doi.org/10.1016/j.jeurceramsoc.2024.01.014.

4 Li, Xudong et al. (2023). Enhanced redox electrocatalysis in high-entropy perovskite fluorides by tailoring D–P hybridization. *Nano-Micro Letters, 16*(1). https://doi.org/10.1007/s40820-023-01275-3.

5 Wang, Yuhao et al. (2023). High-entropy perovskites for Energy Conversion and storage: Design, synthesis, and potential applications. *Small Methods, 7*(4). https://doi.org/10.1002/smtd.202201138.

6 Lisitsyn, Victor, et al. (2023). Radiation synthesis of high-temperature wide-bandgap ceramics. *Micromachines, 14*(12), 2193. https://doi.org/10.3390/mi14122193.

7 Lisitsyn, Victor et al. (2023). The optimization of Radiation Synthesis Modes for YAG: CE Ceramics. *Materials, 16*(8), 3158. https://doi.org/10.3390/ma16083158.

8 Lisitsyn, Victor et al. (2023). Express synthesis of YAG: CE ceramics in the high-energy electrons flow field. *Materials, 16*(3), 1057, https://doi.org/10.3390/ma16031057.

9 Ghyngazov, S.A. et al. (2023). Synthesis of technical ceramics in a beam of fast electrons. *Russian Physics Journal, 66*(4), 391–397, https://doi.org/10.1007/s11182-023-02952-x.

10 NIST Chemistry Webbook, SRD 69. Chemical Formula Search. Retrieved from webbook.nist.gov/chemistry/form-ser/. Accessed 16 Oct. 2024.

11 Glushko, V. (Ed.), Gurvich, L. & et al. (1978, 1979, 1981, 1982). *Termodinamicheskie svoistva individualnykh veshchestv: Spravochnoe izdanie: [V 4-kh tomakh], 3-e izdanie [Thermodynamic Properties of Individual Substances. Reference Edition in 4 Volumes, 3rd Edition]*. Moscow [in Russian].

12 Termodinamicheskie svoistva individualnykh veshchestv: Spravochnoe izdanie. Tom 5 (online versiia) [Thermodynamic Properties of Individual Substances. Reference Edition Volume 5, online version]. Retrieved from https://www.chem.msu.su/rus/tsiv/ [in Russian].

13 Tabata, Tatsuo et al. (1998). An algorithm for depth–dose curves of electrons fitted to Monte Carlo data. *Radiation Physics and Chemistry, 53*(3), 205–215. https://doi.org/10.1016/s0969-806x(98)00102-9.

14 Tabata, Tatsuo et al. (1994). Energy deposition through radiative processes in absorbers irradiated by electron beams. *Nuclear Instruments and Methods in Physics Research Section B: Beam Interactions with Materials and Atoms, 93*(4), 447–456. https://doi.org/10.1016/0168-583x(94)95633-2.

Information about the authors

Golkovski M.G. (corresponding author) — Candidate of physical and mathematical sciences, Senior researcher, Budker Institute of Nuclear Physics, Academician Lavrentiev avenue, 11, Novosibirsk, Russia, e-mail: *golkovski@mail.ru*. ORCID ID: https://orcid.org/0000-0003-4399-444X

Denisov I.P. — Candidate of physical and mathematical sciences, Senior researcher, National Research Tomsk Polytechnic University, Lenin avenue 30, Tomsk, Russia; e-mail: *dip@tpu.ru*

Ghyngazov S.A. — Doctor of technical sciences, Professor, Leading Researcher, National Research Tomsk Polytechnic University, Lenin avenue 30, Tomsk, Russia, e-mail: *ghyngazov@tpu.ru*. https://orcid.org/0000-0002-2524-9238

Vasil'ev I.P. — Candidate of technical science, Senior researcher, National Research Tomsk Polytechnic University, Lenin avenue 30, Tomsk, Russia, e-mail: *zarkvon@tpu.ru*. https://orcid.org/0000-0002-4077-7012

Chakin I.K. — Research Engineer, Budker Institute of Nuclear Physics, Academician Lavrentiev avenue, 11, Novosibirsk, Russia, e-mail: *chak_in2003@bk.ru* ORCID ID: https://orcid.org/0000-0003-0529-2017